Hadron colliders signatures of lepton number violation in the type II seesaw model

Patrick D. Bolton,[1,*] Jonathan Kriewald,[1,†] Miha Nemevšek,[2,1,‡] Fabrizio Nesti,[3,4,§] and Juan Carlos Vasquez[5,‖]

[1]*Jožef Stefan Institute, Jamova 39, 1000 Ljubljana, Slovenia*
[2]*Faculty of Mathematics and Physics, University of Ljubljana, Jadranska 19, 1000 Ljubljana, Slovenia*
[3]*Dipartimento di Scienze Fisiche e Chimiche, Università dell'Aquila, via Vetoio, I-67100, L'Aquila, Italy*
[4]*INFN, Laboratori Nazionali del Gran Sasso, I-67100 Assergi (AQ), Italy*
[5]*Department of Physics and Astronomy, Science Center, Amherst College, Amherst, Massachusetts 01002, USA*

(Received 29 August 2024; accepted 17 January 2025; published 18 February 2025)

We examine the prospect of observing genuine lepton-number-violating (LNV) signals at hadron colliders in the context of the type II seesaw mechanism. The model features smoking gun signals involving same-sign di-leptons and jets that may be the primary observable channel in certain regions of the parameter space. The flavor composition of final-state charged leptons is related to the origin of neutrino masses and is correlated with other rare processes, such as neutrinoless double-beta decay. We review existing collider limits and provide sensitivity estimates from LNV signals at upcoming Large Hadron Collider runs, including nonzero mass splittings between triplet components.

DOI: 10.1103/PhysRevD.111.035016

I. INTRODUCTION

A well-known feature of the standard model (SM) is the accidental conservation of the total lepton number L. The observation of nonzero neutrino masses could imply the existence of L-number-violating (LNV) new physics. According to Majorana [1], a real representation under the Lorentz group can describe neutrinos with a $\Delta L = 2$ mass term. The most studied LNV process, sensitive to light neutrino exchange and new physics, is neutrinoless double-beta decay ($0\nu\beta\beta$) [2]. Considerable experimental and theoretical efforts are underway to detect such smoking gun signals and establish their connection to light neutrinos [3] and new physics [4] (for a review, see [5]).

Other LNV processes have been probed from eV to beyond TeV [6]. Perhaps the most striking signature is the final state of two same-sign charged leptons and two jets in pp collisions, arising from the production and decay of heavy Majorana neutrinos N. Such states are the key ingredient of type I seesaw scenarios [7–11], which can introduce Majorana masses m_N for the gauge singlets ν_R either by hand or via the spontaneous symmetry breaking of an extended gauge group, such as in the minimal left-right symmetric model (LRSM) [8,12–14]. There, it is tied to the scale of $SU(2)_R$ breaking through the Yukawa coupling Y_N as $m_N = Y_N v_R$, where v_R is the vacuum expectation value (VEV) of the scalar triplet Δ_R.

In models with gauged $U(1)_{B-L}$ [and $SU(2)_R$], the VEV v_R can be in the TeV range, kinematically accessible to colliders. Distinct LNV signatures, such as the Keung-Senjanović [15] channel, appear nearly automatically due to the presence of m_N and Yukawa couplings that communicate LNV to the SM. The production and decay of on-shell N via charged currents leads to LNV in half of the events, containing two same-sign leptons and jets. In the case of interference, the ratio of same- and opposite-sign leptons may be altered [16] and LNV may be suppressed by pseudo-Dirac masses [17,18]. The exact origin of heavy Majorana neutrino masses can be determined from complementary signals, such as the Higgs decay $h \to NN$ via the $h - \Delta_R^0$ mixing [19,20], which can also feature LNV final states with two same-sign leptons and up to four jets. See [21] for a review of the LRSM parameter space and [22] for future colliders.

The type II seesaw [23–27] provides Majorana masses for the light neutrinos without extending the SM gauge group or fermion content. A single scalar triplet $\Delta_L = (3, 2)$ under $SU(2)_L \otimes U(1)_Y$ can partially break the electroweak (EW) symmetry with its VEV v_Δ. The Yukawa term that couples the left-handed lepton doublet to the triplet with the

*Contact author: patrick.bolton@ijs.si
†Contact author: jonathan.kriewald@ijs.si
‡Contact author: miha.nemevsek@ijs.si
§Contact author: fabrizio.nesti@aquila.infn.it
‖Contact author: jvasquezcarm@umass.edu

coupling Y_Δ then leads to the Majorana neutrino mass matrix $M_\nu \propto Y_\Delta v_\Delta$.

The production of charged and neutral scalars in the model proceeds through the EW interactions [28,29], followed by decays defining the final state [30–34]. For $v_\Delta \lesssim 10$ keV, leptonic decay modes dominate with three- and four-lepton states, with current flavor-dependent lower bounds on the doubly charged scalar mass in the $\mathcal{O}(500\text{–}700)$ GeV range [35–41]. In such final states, the total lepton number is conserved (LNC). Another LNC search exists in the $v_\Delta \gtrsim 100$ keV region, where decays to SM vector bosons take over, with weaker bounds at $m_{\Delta^{++}} \gtrsim 350$ GeV [42–44]. Mass splittings between Δ_L components trigger LNC cascade decays [45,46] that either enhance or reduce the bounds. Signatures of type II have been investigated at future lepton [47], $e-p$ [48], and hadron [49,50] colliders.

It is well known [51] that genuine LNV signals in type II require the simultaneous presence of Y_Δ and v_Δ. Turning on the Yukawa coupling Y_Δ ensures that the Δ_L triplet indeed has $L=2$. Then, v_Δ communicates $L \neq 0$ to the SM sector with $L=0$ and the combined effect leads to LNV. This is especially obvious when the final-state gauge bosons decay hadronically and neutrinos cannot carry away L. In pure type II, the product $Y_\Delta v_\Delta$ is fixed and LNV signals are not automatically observable.

The LNV window [51] exists for $v_\Delta \simeq 10\text{–}100$ keV, where both decay modes, proportional to Y_Δ and v_Δ, are present. Smoking gun signals with two same-sign leptons and jets appear, as shown in Fig. 1. While existing leptonic searches can be recast to the LNV region [52,53] with some sensitivity, the dedicated analysis presented here opens the LNV window completely, and accounts for the presence of mass splittings in Δ_L. We determine the strength of the LNV signal with a di-lepton plus jets analysis that significantly improves the sensitivity, spanning the range of v_Δ shown in Fig. 2.

II. LOCATION OF THE LNV WINDOW

In the type II seesaw, the Yukawa term

$$\mathcal{L}_{\rm Yuk} \supset -Y_{\Delta ij} L_i^T \mathcal{C} i\sigma_2 \Delta_L L_j + \text{H.c.}, \tag{1}$$

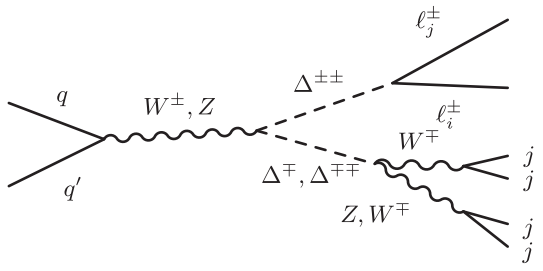

FIG. 1. Pair (and associated) production of charged scalars mediated by Z/γ^* ($W^\pm$), producing the LNV final state $\ell^\pm\ell'^\pm 4j$ at the LHC.

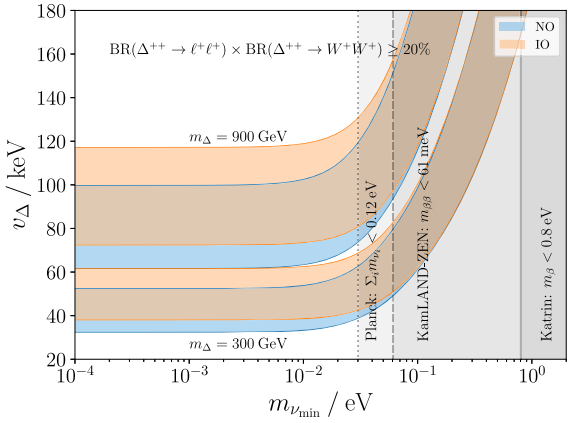

FIG. 2. Position of the LNV window in the type II seesaw, defined by $\mathrm{BR}_{\Delta^{++}\to\ell^+\ell^+} \times \mathrm{BR}_{\Delta^{++}\to W^+W^+} > 20\%$. Blue and orange bands correspond to the normal hierarchy (NO) and inverted hierarchy (IO) cases, each with the benchmark masses $m_{\Delta^{++}} = 300$ GeV and 900 GeV. The gray regions indicate the limits from Planck data [54] (dotted vertical line), $0\nu\beta\beta$ from KamLAND-Zen [55] (dashed line), and KATRIN [56] (solid line).

with

$$\Delta_L = \begin{pmatrix} \Delta^+/\sqrt{2} & \Delta^{++} \\ (v_\Delta + \Delta^0 + i\chi_\Delta)/\sqrt{2} & -\Delta^+/\sqrt{2} \end{pmatrix}, \tag{2}$$

sources the light neutrino mass matrix

$$M_\nu = V^* m_\nu V^\dagger = \sqrt{2} Y_\Delta v_\Delta, \tag{3}$$

where $m_\nu = \mathrm{diag}(m_1, m_2, m_3)$ contains the light neutrino masses and V is the Pontecorvo-Maki-Nakagawa-Sakata mixing matrix. The singly charged Δ^+ and pseudoscalar χ_Δ components mix with the SM would-be Goldstones, while the neutral component Δ^0 mixes with the SM Higgs h with a small mixing of order v_Δ/v. Equation (1) also results in the decays of Δ^{++} to two same-sign charged leptons, with

$$\Gamma_{\Delta^{++}\to\ell_i^+\ell_j^+} = \frac{m_{\Delta^{++}}}{8\pi(1+\delta_{ij})}\left|\frac{M_{\nu ij}}{v_\Delta}\right|^2, \tag{4}$$

where δ_{ij} is the Kronecker delta. Through M_ν, and hence m_ν and V, these rates are directly related to neutrino oscillations [30–32]. The total leptonic rate, $\Gamma_{\Delta^{++}\to\ell^+\ell^+} = m_{\Delta^{++}}/(16\pi)\sum m_\nu^2/v_\Delta^2$, is insensitive to V and depends only on the neutrino masses, determined from the mass-squared differences Δm_{21}^2 and Δm_{32}^2 and the lightest neutrino mass $m_{\nu_{\rm min}}$. With m_ν fixed by oscillations, the leptonic rates in Eq. (4) dominate the $\Gamma^{\rm tot}_{\Delta^{++}}$ when v_Δ becomes small, until the lower bound on v_Δ is met, coming from the nonobservation of lepton-flavor-violating (LFV) processes [57–62] and Y_Δ perturbativity. For the larger values of v_Δ relevant for the LNV window, the LFV rates are highly

suppressed by small Yukawa couplings and the constraints become irrelevant.

Likewise, $v_\Delta \neq 0$ triggers decays of Δ_L components into the SM gauge bosons via the kinetic term $\mathrm{Tr}[(D_\mu \Delta_L)^\dagger (D^\mu \Delta_L)]$. Particularly important are the decays $\Delta^{++} \to W^+W^+$ and $\Delta^+ \to W^+Z$, with the rates

$$\Gamma_{\{W^+W^+, W^+Z\}} \simeq \frac{\alpha_2}{4}\left(\frac{v_\Delta}{v}\right)^2 \left\{\frac{m^3_{\Delta^{++}}}{M_W^2}, \frac{m^3_{\Delta^+}}{2M_W^2}\right\}, \tag{5}$$

for $m_{\Delta^+}, m_{\Delta^{++}} \gg v$. Also relevant are $\Delta^+ \to W^+h$ and $\Delta^+ \to t\bar{b}$ that proceed via $\Delta^+ - \chi^+$ mixing, with

$$\Gamma_{\Delta^+ \to W^+h} \simeq \frac{\alpha_2}{8}\left(\frac{v_\Delta}{v}\right)^2 \frac{m^3_{\Delta^+}}{M_W^2}, \tag{6}$$

$$\Gamma_{\Delta^+ \to t\bar{b}} \simeq \frac{3}{4\pi}\left(\frac{v_\Delta}{v}\right)^2 m_{\Delta^+}\left(\frac{m_t}{v}\right)^2. \tag{7}$$

Unlike Eq. (4), these are independent of m_ν and dominate for larger values of v_Δ. The upper bound of $v_\Delta \lesssim \mathcal{O}(1)$ GeV comes from electroweak precision tests (EWPTs).

The number of genuine LNV signal events is proportional to the product of leptonic and gauge branching ratios, $\mathrm{BR}_{\Delta^{++}\to\ell\ell} \times \{\mathrm{BR}_{\Delta^{++}\to WW}, \mathrm{BR}_{\Delta^+\to WZ(h)}$, and $\mathrm{BR}_{\Delta^+\to t\bar{b}}\}$ that define the LNV window. Its position depends on the neutrino mass ordering but less so on $m_{\nu_{\min}}$, and nontrivial behavior happens in the region disfavored by the cosmological data [54] and the latest $0\nu\beta\beta$ [55] and KATRIN [56] searches. The exact location is shown in Figs. 2 and 3 and depends nontrivially on $m_{\Delta^{++}}$, which we scan within the Large Hadron Collider (LHC) observable range. It is maximal for $v_\Delta \sim 40$–50 keV.

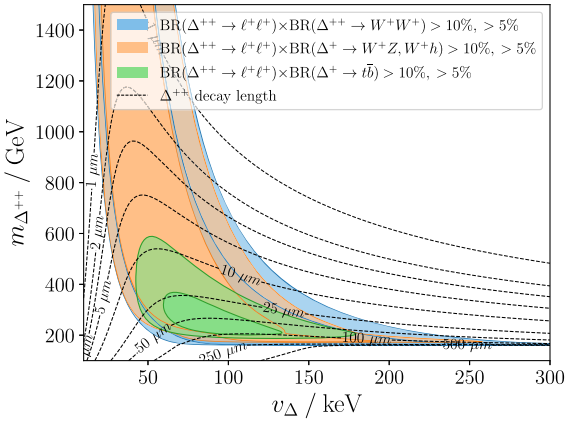

FIG. 3. Regions with the branching ratios of $\mathrm{BR}_{\Delta^{\pm\pm}\to\ell^\pm\ell^\pm} \times \{\mathrm{BR}_{\Delta^{\pm\pm}\to W^\pm W^\pm}, \mathrm{BR}_{\Delta^\pm\to W^\pm Z(h)}$, and $\mathrm{BR}_{\Delta^\pm\to t\bar{b}}\} > 5\%$ and 10% in blue, orange, and green. The NO mass spectrum is assumed with $m_{\nu_{\min}} = 0.01$ eV. The dashed lines show the Δ^{++} decay length in the rest frame, see [63–66] for displacement.

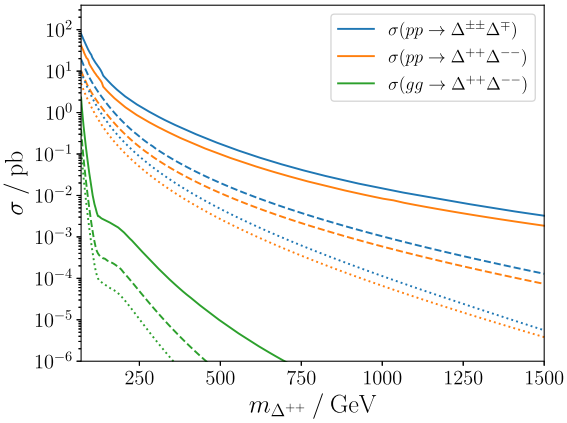

FIG. 4. Proton-level cross sections at $\sqrt{s} = 14$, 27, and 100 TeV in dotted, dashed, and solid lines, with $\Delta m = 0$, for the LO-associated, EW pair, and gluon fusion Higgs pair production.

III. SIZE OF THE LNV WINDOW

To obtain the number of LNV events, the branching ratios above are multiplied by the dominant production cross sections. The doubly charged scalars can be pair-produced in pp collisions through off-shell $\gamma/Z/h \to \Delta^{\pm\pm}\Delta^{\mp\mp}$ and in the associated channel via $W^\pm \to \Delta^{\pm\pm}\Delta^\mp$ (see Fig. 1). The associated production cross section is integrated over the parton distribution functions (PDFs) as

$$\sigma^{\mathrm{LO}}_{\mathrm{assoc}} \simeq \int_{\mathrm{PDF}} \frac{\pi\alpha_2^2}{36} \frac{\hat{s}(1 - 4m^2_{\Delta^{++}}/\hat{s})^{3/2}}{(\hat{s} - M_W)^2 + (\Gamma_W M_W)^2}, \tag{8}$$

and similarly for $\gamma/Z/h$ exchange. The leading order (LO) cross sections at different $\sqrt{s}$, multiplied by the next-to-leading-order (NLO) K-factors, are shown in Fig. 4. We assumed $m_{\Delta^{++}} = m_{\Delta^+} = m_{\Delta^0}$, and the impact of mass splittings is discussed below. For details of NLO cross sections and PDF uncertainties, see [29,67]. The kinematics of NLO jet emissions does not impact our study, and the LO simulations are sufficient for an accurate estimate of signal selection efficiencies in the LNV window.

IV. SENSITIVITY AT THE LHC

To enhance the sensitivity to the type II LNV window, we propose the following search, based on Monte Carlo simulations of the $\ell^\pm\ell'^\pm$ + jets' final states for the signal and backgrounds at the LHC. We focus on three possible electron and muon final states: $e^\pm e^\pm$, $\mu^\pm\mu^\pm$, and the $e^\pm\mu^\pm$ LFV channel.

We use the FeynRules [68] implementation of the model file [29] for the generation of signal events in the MadGraph5 [69] framework at LO. Pythia8 [70] is used for showering and hadronization and the DELPHES [71] library for fast detector simulation, using the default detector cards. We use MadAnalysis5 [72] for designing and implementing the

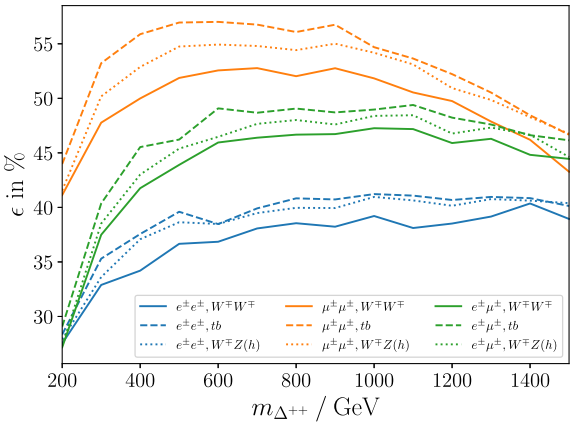

FIG. 5. Efficiencies after selection cuts for the signal events in the $\ell^\pm\ell^\pm W^\mp W^\mp$, $\ell^\pm\ell^\pm W^\mp Z(h)$ and $\ell^\pm\ell^\pm tb$ channels.

following cuts. We select events with at least two same-sign leptons, $\ell^\pm\ell'^\pm$, $\ell, \ell' = e, \mu$, and at least two jets, defined with the anti-k_T algorithm using $\Delta R = 0.3$ and $p_{Tj\,\mathrm{min}} = 20$ GeV. We impose cuts of $p_{T\ell} > 50$ GeV and $p_{Tj} > 50$ GeV on the leading lepton and jet. Then, we accept events within the narrow di-lepton invariant mass peak, $m_{\ell\ell} \in [0.9, 1.1] m_{\Delta^{++}}$, and reject those with $\Delta R_{\ell\ell} > \pi$. Events with the invariant mass $m_{j_1 j_2} > 1.1 m_{\Delta^{++}}$ for the two leading jets are omitted.

Figure 5 shows the signal efficiencies, i.e., ratios between the number of events after applying the cuts and the initial number of simulated events with hadronically decaying $V = W^\pm, Z$.

The main sources of background are $V + 012js$, $VV + 012js$, and $t\bar{t} + 012js$. All simulations were performed with aMC@NLO at LO with up to two matched jets and rescaled to the NLO cross sections.

The estimated sensitivities $\mathcal{S}$, used to establish upper limits for the LNV channels, are obtained with $\mathcal{S}^2 = \sum_i s_i^2/(s_i + b_i)$, where $s_i(b_i)$ is the expected number of signal (background) events in each region i after cuts. They are shown in Fig. 6, together with the exclusion regions of current searches by ATLAS, CMS, L3, and OPAL [35–43] in purple. We omit the inclusive ATLAS search [73], where all flavor channels were combined into a single sensitivity. The bounds from current searches in the leptonic channels (purple) in Fig. 6 disappear at around $v_\Delta \sim 100$ keV, while for $v_\Delta > 200$ keV, the $W^\pm W^\pm$ channel takes over, with a weaker exclusion of $m_{\Delta^{++}} \gtrsim 350$ GeV (rose).

In the intermediate v_Δ range, both leptonic and gauge searches are weakened, and the opportunity for *genuine* LNV signals emerges. Sensitivity estimates reveal encouraging prospects justified by the extent of the LNV windows in Fig. 6. They cover a large portion of parameter space, above the limits of existing searches and spanning orders of magnitude in v_Δ.

V. IMPACT OF MASS SPLITTINGS

The scalar potential contains two bi-quadratic terms that couple Δ_L to the Higgs doublet φ,

$$\lambda_{h\Delta 1}\varphi^\dagger\varphi \mathrm{Tr}\left[\Delta_L^\dagger \Delta_L\right] + \lambda_{h\Delta 2}\mathrm{Tr}\left[\varphi\varphi^\dagger \Delta_L \Delta_L^\dagger\right]. \tag{9}$$

The $\lambda_{h\Delta 1}$ gives a universal mass shift to all triplet scalar components and is limited by $h \to \gamma\gamma$, while the $\lambda_{h\Delta 2}$ term splits them, such that

$$m_{\Delta^0}^2 - m_{\Delta^+}^2 = m_{\Delta^+}^2 - m_{\Delta^{++}}^2 = \frac{\lambda_{h\Delta 2} v^2}{4}, \tag{10}$$

up to $\mathcal{O}(v_\Delta/v)^2$. The perturbativity bound $\lambda_{h\Delta 2} \lesssim \sqrt{4\pi}$ limits the size of the mass splitting, especially for larger $m_{\Delta^{++}}$. For smaller values of $m_{\Delta^{++}}$, the EWPT oblique parameters [45,74–77] further constrain the splitting, as

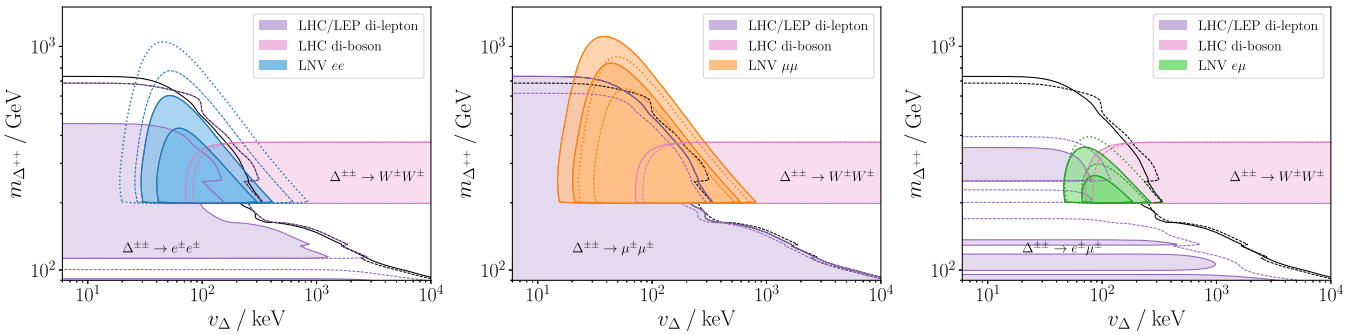

FIG. 6. The LNV window sensitivity at $\sqrt{s} = 14$ TeV for pair and associated production of Δ^{++} with $m_{\nu_{\mathrm{min}}} = 0.01$ eV. The left, center, and right panels correspond to the combined $e^\pm e^\pm 4j$, $\mu^\pm\mu^\pm 4j$, and $e^\pm\mu^\pm 4j$ channels. The inner (outer) regions correspond to $\mathcal{L} = 300$ fb^{-1} (3000 fb^{-1}), and solid lines show the sensitivity at 2σ for NO. The dashed (dotted) lines denote the sensitivity for IO at 300 fb^{-1} (3000 fb^{-1}). The black solid (dashed) lines denote the strongest bound from exclusive flavor channels for NO (IO). The purple region shows the exclusion from the doubly charged searches in the di-lepton channel(s) [35–41]. The rose region denotes the $\Delta^{\pm\pm} \to W^\pm W^\pm$ and $\Delta^{\pm\pm}, \Delta^\mp \to W^\pm W^\pm$, and $W^\mp Z$ searches [42,43].

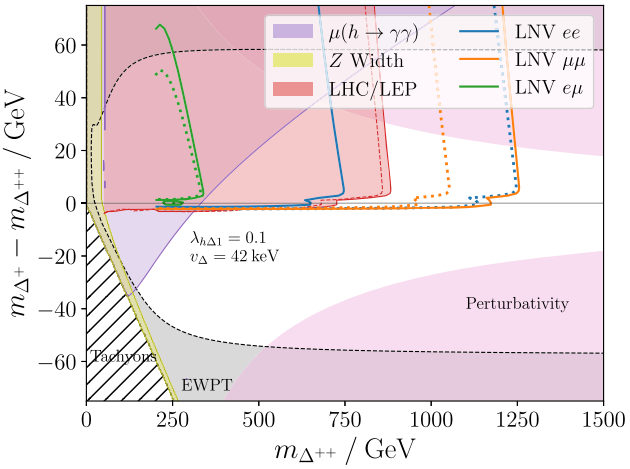

FIG. 7. Future sensitivity of the LHC to the LNV window for NO (IO) in solid (dotted) lines, with $\mathcal{L} = 3000$ fb^{-1}. Blue, orange, and green lines denote the $e^\pm e^\pm$, $\mu^\pm\mu^\pm$, and $e^\pm\mu^\pm$ channels. The gray area shows the EWPT constraints, the pink region excludes $\lambda_{h\Delta 2} > \sqrt{4\pi}$, the light green region shows the $\Gamma_Z^{\rm tot}$, the purple region shows $h \to \gamma\gamma$, and the red region current direct searches, as in Fig. 6. The hatched area is forbidden by the sum rule (10).

shown in Fig. 7 (see [75,78] for details). As realized in [45], mass splittings trigger three-body cascades via off-shell V, such as $\Delta^{++} \to \Delta^+ f\bar{f}$, approximated by

$$\Gamma_{\Delta^{++}\to\Delta^+ f\bar{f}} \simeq \frac{3\alpha_2^2}{5\pi}\frac{\Delta m^5}{M_W^4}, \tag{11}$$

with $\Delta m = m_{\Delta^{++}} - m_{\Delta^+}$. Two-body cascades require a large mass splitting $\Delta m > M_{W,Z}$ and are disfavored by EWPT—only off-shell Vs with soft leptons and jets are relevant.

Cascade decays modify the number of LNV events coming from the pair or associated production of Δ_L. Additional sources of same-sign charged leptons are present when Δ^{++} is the lightest, coming from the production and cascade decays of $\Delta^{+,0}$. When Δ^{++} is the heaviest, the $\Delta^{\pm\pm} \to \ell^\pm\ell'^\pm$ final state is suppressed by cascades to $\Delta^{+,0}$, whose decay products fail to pass the invariant mass cut on $m_{\ell^\pm\ell'^\pm}$. The resulting sensitivity, together with current bounds from direct searches and the indirect constraints outlined above, is shown in Fig. 7 (see also cascades sensitivities at the LHC [79,80] and e^+e^- colliders [81]).

VI. CONCLUSIONS AND OUTLOOK

We investigated the prospect of observing LNV signals in the minimal type II seesaw and delineated the region of parameter space where the sensitivity of current LNC searches diminishes and a genuine LNV signal becomes observable. Our selection criteria strongly reduced the known SM backgrounds and enhanced the sensitivity, revealing encouraging prospects for searches at hadron colliders, filling the remaining gap in current searches.

The Δ_L also appears in the LRSM [26], where the mass splittings are large if M_{W_R} was fairly light [82], leading to a lower bound for $m_{\Delta^{++}}$ at around 1 TeV if W_R was accessible at the LHC (see also [83]). The LRSM seesaw extends (3) with another Type I source, spoiling the relation between Y_Δ and v_Δ and modifying the flavour structure of final-state leptons. This shifts the location of the LNV window, whereas the kinematics and estimated efficiencies still apply. The future outlook for enhancing the sensitivity of the LNV window includes the τ final states, leptonic decays of $W^\pm$ and Z, and Δ^0, χ_Δ contributions. Interest in the LNV window may be spurred by cosmology, where Type II can play an important role in phase transitions [84,85] and leptogenesis. While the standard leptogenesis scenario with a single Δ_L fails [86], a successful variant was claimed in [87,88]. The washout effects are strongest precisely within the LNV window [89].

ACKNOWLEDGMENTS

M. N. would like to thank Yue Zhang and Richard Ruiz for discussions. P. D. B., J. K., and M. N. are supported by the Slovenian Research Agency under the research core funding No. P1-0035, and in part by the research Grants No. J1-3013 and No. N1-0253. M. N. is grateful to the Mainz Institute for Theoretical Physics (MITP) of the DFG Cluster of Excellence PRISMA+ (Project ID 33083149) for its hospitality and its partial support during the course of this work. P. D. B. , J. K., M. N., and F. N. thank the CERN Theory group for their hospitality, during which a part of the work was being done. M. N. thanks the Carleton University for the hospitality and support during the completion of the paper. J. C. V. would like to thank Goran Senjanović and Michael Ramsey-Musolf for the encouragement and enlightening discussions. J. C. V. was partially funded under the US Department of Energy Contract No. DE-SC0011095.

[1] E. Majorana, Nuovo Cimento **14**, 171 (1937).
[2] G. Racah, Nuovo Cimento **14**, 322 (1937).
[3] F. Vissani, J. High Energy Phys. 06 (1999) 022.
[4] V. Tello, M. Nemevšek, F. Nesti, G. Senjanović, and F. Vissani, Phys. Rev. Lett. **106**, 151801 (2011).
[5] M. J. Dolinski, A. W. P. Poon, and W. Rodejohann, Annu. Rev. Nucl. Part. Sci. **69**, 219 (2019).
[6] Y. Cai, T. Han, T. Li, and R. Ruiz, Front. Phys. **6**, 40 (2018).
[7] P. Minkowski, Phys. Lett. **67B**, 421 (1977).
[8] R. N. Mohapatra and G. Senjanović, Phys. Rev. Lett. **44**, 912 (1980).
[9] S. L. Glashow, NATO Sci. Ser. B **61**, 687 (1980).
[10] M. Gell-Mann, P. Ramond, and R. Slansky, Conf. Proc. C **790927**, 315 (1979), https://inspirehep.net/literature/9686.
[11] T. Yanagida, Conf. Proc. C **7902131**, 95 (1979), https://inspirehep.net/literature/143150.
[12] J. C. Pati and A. Salam, Phys. Rev. D **10**, 275 (1974); **11**, 703(E) (1975).
[13] R. N. Mohapatra and J. C. Pati, Phys. Rev. D **11**, 566 (1975).
[14] G. Senjanovic and R. N. Mohapatra, Phys. Rev. D **12**, 1502 (1975).
[15] W.-Y. Keung and G. Senjanović, Phys. Rev. Lett. **50**, 1427 (1983).
[16] J. Gluza, T. Jelinski, and R. Szafron, Phys. Rev. D **93**, 113017 (2016).
[17] J. Kersten and A. Y. Smirnov, Phys. Rev. D **76**, 073005 (2007).
[18] M. Drewes, J. Klarić, and P. Klose, J. High Energy Phys. 11 (2019) 032.
[19] A. Maiezza, M. Nemevšek, and F. Nesti, Phys. Rev. Lett. **115**, 081802 (2015).
[20] M. Nemevšek, F. Nesti, and J. C. Vasquez, J. High Energy Phys. 04 (2017) 114.
[21] M. Nemevšek, F. Nesti, and G. Popara, Phys. Rev. D **97**, 115018 (2018).
[22] M. Nemevšek and F. Nesti, Phys. Rev. D **108**, 015030 (2023).
[23] M. Magg and C. Wetterich, Phys. Lett. **94B**, 61 (1980).
[24] J. Schechter and J. W. F. Valle, Phys. Rev. D **22**, 2227 (1980).
[25] T. P. Cheng and L.-F. Li, Phys. Rev. D **22**, 2860 (1980).
[26] R. N. Mohapatra and G. Senjanović, Phys. Rev. D **23**, 165 (1981).
[27] G. Lazarides, Q. Shafi, and C. Wetterich, Nucl. Phys. **B181**, 287 (1981).
[28] T. Han, B. Mukhopadhyaya, Z. Si, and K. Wang, Phys. Rev. D **76**, 075013 (2007).
[29] B. Fuks, M. Nemevšek, and R. Ruiz, Phys. Rev. D **101**, 075022 (2020).
[30] E. J. Chun, K. Y. Lee, and S. C. Park, Phys. Lett. B **566**, 142 (2003).
[31] J. Garayoa and T. Schwetz, J. High Energy Phys. 03 (2008) 009.
[32] M. Kadastik, M. Raidal, and L. Rebane, Phys. Rev. D **77**, 115023 (2008).
[33] P. Fileviez Perez, T. Han, G.-y. Huang, T. Li, and K. Wang, Phys. Rev. D **78**, 015018 (2008).
[34] A. Das, P. Das, and N. Okada, arXiv:2405.11820.
[35] M. Aaboud *et al.* (ATLAS Collaboration), Eur. Phys. J. C **78**, 199 (2018).
[36] S. Chatrchyan *et al.* (CMS Collaboration), Eur. Phys. J. C **72**, 2189 (2012).
[37] P. Achard *et al.* (L3 Collaboration), Phys. Lett. B **576**, 18 (2003).
[38] G. Aad *et al.* (ATLAS Collaboration), J. High Energy Phys. 08 (2015) 138.
[39] G. Abbiendi *et al.* (OPAL Collaboration), Phys. Lett. B **526**, 221 (2002).
[40] CMS Collaboration, A search for doubly-charged Higgs boson production in three and four lepton final states at $\sqrt{s} = 13$ TeV, Technical Report, CERN, Geneva, 2017.
[41] G. Aad *et al.* (ATLAS Collaboration), J. High Energy Phys. 03 (2015) 041.
[42] G. Aad *et al.* (ATLAS Collaboration), J. High Energy Phys. 06 (2021) 146.
[43] M. Aaboud *et al.* (ATLAS Collaboration), Eur. Phys. J. C **79**, 58 (2019).
[44] G. Aad *et al.* (ATLAS Collaboration), arXiv:2405.04914.
[45] A. Melfo, M. Nemevšek, F. Nesti, G. Senjanović, and Y. Zhang, Phys. Rev. D **85**, 055018 (2012).
[46] R. Primulando, J. Julio, and P. Uttayarat, J. High Energy Phys. 08 (2019) 024.
[47] P. Agrawal, M. Mitra, S. Niyogi, S. Shil, and M. Spannowsky, Phys. Rev. D **98**, 015024 (2018).
[48] P. S. B. Dev, S. Khan, M. Mitra, and S. K. Rai, Phys. Rev. D **99**, 115015 (2019).
[49] Y. Du, A. Dunbrack, M. J. Ramsey-Musolf, and J.-H. Yu, J. High Energy Phys. 01 (2019) 101.
[50] R. Padhan, D. Das, M. Mitra, and A. Kumar Nayak, Phys. Rev. D **101**, 075050 (2020).
[51] A. Maiezza, M. Nemevšek, and F. Nesti, AIP Conf. Proc. **1743**, 030008 (2016).
[52] F. del Águila and M. Chala, J. High Energy Phys. 03 (2014) 027.
[53] K. S. Babu, R. K. Barman, D. Gonçalves, and A. Ismail, J. High Energy Phys. 06 (2024) 132.
[54] N. Aghanim *et al.* (Planck Collaboration), Astron. Astrophys. **641**, A6 (2020); **652**, C4(E) (2021).
[55] A. Gando *et al.* (KamLAND-Zen Collaboration), Phys. Rev. Lett. **117**, 082503 (2016); **117**, 109903(A) (2016).
[56] M. Aker *et al.* (KATRIN Collaboration), Nat. Phys. **18**, 160 (2022).
[57] A. Abada, C. Biggio, F. Bonnet, M. B. Gavela, and T. Hambye, J. High Energy Phys. 12 (2007) 061.
[58] T. Fukuyama, H. Sugiyama, and K. Tsumura, J. High Energy Phys. 03 (2010) 044.
[59] P. S. B. Dev, M. J. Ramsey-Musolf, and Y. Zhang, Phys. Rev. D **98**, 055013 (2018).
[60] N. D. Barrie and S. T. Petcov, J. High Energy Phys. 01 (2023) 001.
[61] M. Ardu, S. Davidson, and S. Lavignac, J. High Energy Phys. 11 (2023) 101.
[62] U. Banerjee, C. Englert, and W. Naskar, Phys. Rev. D **110**, 055010 (2024).
[63] P. S. Bhupal Dev and Y. Zhang, J. High Energy Phys. 10 (2018) 199.

[64] S. Antusch, O. Fischer, A. Hammad, and C. Scherb, J. High Energy Phys. 02 (2019) 157.
[65] J. Alimena *et al.*, J. Phys. G **47**, 090501 (2020).
[66] C. Arbeláez, J. C. Helo, and M. Hirsch, Phys. Rev. D **100**, 055001 (2019).
[67] M. Muhlleitner and M. Spira, Phys. Rev. D **68**, 117701 (2003).
[68] A. Alloul, N. D. Christensen, C. Degrande, C. Duhr, and B. Fuks, Comput. Phys. Commun. **185**, 2250 (2014).
[69] J. Alwall, R. Frederix, S. Frixione, V. Hirschi, F. Maltoni, O. Mattelaer, H. S. Shao, T. Stelzer, P. Torrielli, and M. Zaro, J. High Energy Phys. 07 (2014) 079.
[70] T. Sjostrand, S. Mrenna, and P. Z. Skands, Comput. Phys. Commun. **178**, 852 (2008).
[71] J. de Favereau, C. Delaere, P. Demin, A. Giammanco, V. Lemaître, A. Mertens, and M. Selvaggi (DELPHES 3 Collaboration), J. High Energy Phys. 02 (2014) 057.
[72] E. Conte, B. Fuks, and G. Serret, Comput. Phys. Commun. **184**, 222 (2013).
[73] G. Aad *et al.* (ATLAS Collaboration), Eur. Phys. J. C **83**, 605 (2023).
[74] M. E. Peskin and T. Takeuchi, Phys. Rev. D **46**, 381 (1992).
[75] L. Lavoura and L.-F. Li, Phys. Rev. D **49**, 1409 (1994).
[76] E. J. Chun, H. M. Lee, and P. Sharma, J. High Energy Phys. 11 (2012) 106.
[77] J. Haller, A. Hoecker, R. Kogler, K. Mönig, T. Peiffer, and J. Stelzer, Eur. Phys. J. C **78**, 675 (2018).
[78] Y. Cheng, X.-G. He, F. Huang, J. Sun, and Z.-P. Xing, Nucl. Phys. **B989**, 116118 (2023).
[79] S. Ashanujjaman and K. Ghosh, J. High Energy Phys. 03 (2022) 195.
[80] S. Ashanujjaman and S. P. Maharathy, Phys. Rev. D **107**, 115026 (2023).
[81] S. Ashanujjaman, K. Ghosh, and K. Huitu, Phys. Rev. D **106**, 075028 (2022).
[82] A. Maiezza, M. Nemevšek, and F. Nesti, Phys. Rev. D **94**, 035008 (2016).
[83] J. Gluza, M. Kordiaczynska, and T. Srivastava, Chin. Phys. C **45**, 073113 (2021).
[84] R. Zhou, L. Bian, and Y. Du, J. High Energy Phys. 08 (2022) 205.
[85] P. Ghosh, T. Ghosh, and S. Roy, J. High Energy Phys. 10 (2023) 057.
[86] T. Hambye and G. Senjanović, Phys. Lett. B **582**, 73 (2004).
[87] N. D. Barrie, C. Han, and H. Murayama, Phys. Rev. Lett. **128**, 141801 (2022).
[88] N. D. Barrie, C. Han, and H. Murayama, J. High Energy Phys. 05 (2022) 160.
[89] S. Blanchet, Z. Chacko, and R. N. Mohapatra, Phys. Rev. D **80**, 085002 (2009).